

Article

Anomaly Negative Resistance Phenomena in Highly Epitaxial PrBa_{0.7}Ca_{0.3}Co₂O_{5+δ} Thin Films Induced from Superfast Redox Reactions

Yumei Luo^{1,2}, Xing Xu^{2,3}, Yudong Xia^{2,4}, Shengli Pang^{2,5} , Fen Xu¹, Myung-Hwan Whangbo^{6,7} , Lixian Sun^{1,*}  and Chonglin Chen^{2,*}

- ¹ Guangxi Collaborative Innovation Center of Structure and Property for New Energy, Guangxi Key Laboratory of Information Materials, Guilin University of Electronic Technology, Guilin 541004, China; luoym@guet.edu.cn (Y.L.); xufen@guet.edu.cn (F.X.)
- ² Department of Physics and Astronomy, University of Texas at San Antonio, San Antonio, TX 78249, USA; xuxing@mail.tsinghua.edu.cn (X.X.); Ydxia@swjtu.edu.cn (Y.X.); slpang@ujs.edu.cn (S.P.)
- ³ School of Physics and Electronic Information, Gannan Normal University, Ganzhou 341000, China
- ⁴ School of Physical Science and Technology, Southwest Jiaotong University, Chengdu 611756, China
- ⁵ Institute for Advanced Materials, Jiangsu University, Zhenjiang 212013, China
- ⁶ Department of Chemistry, North Carolina State University, Raleigh, NC 27695, USA; whangbo@ncsu.edu
- ⁷ State Key Laboratory of Structural Chemistry, Fujian Institute of Research on the Structure of Matter (FJIRSM), Chinese Academy of Sciences (CAS), Fuzhou 350002, China
- * Correspondence: sunlx@guet.edu.cn (L.S.); Chonglin.Chen@utsa.edu (C.C.)



Citation: Luo, Y.; Xu, X.; Xia, Y.; Pang, S.; Xu, F.; Whangbo, M.-H.; Sun, L.; Chen, C. Anomaly Negative Resistance Phenomena in Highly Epitaxial PrBa_{0.7}Ca_{0.3}Co₂O_{5+δ} Thin Films Induced from Superfast Redox Reactions. *Catalysts* **2021**, *11*, 1441. <https://doi.org/10.3390/catal11121441>

Academic Editor:
Stanislaw Waclawek

Received: 31 October 2021
Accepted: 22 November 2021
Published: 26 November 2021

Publisher's Note: MDPI stays neutral with regard to jurisdictional claims in published maps and institutional affiliations.



Copyright: © 2021 by the authors. Licensee MDPI, Basel, Switzerland. This article is an open access article distributed under the terms and conditions of the Creative Commons Attribution (CC BY) license (<https://creativecommons.org/licenses/by/4.0/>).

Abstract: Thin films of Ca-doped double perovskite, PrBa_{0.7}Ca_{0.3}Co₂O_{5+δ} (PBCC), were epitaxially grown on (001) SrTiO₃, and their redox reactions under a switching flow of H₂ and O₂ gases were examined at various temperatures by measuring the resistance R(t) of the films as a function of the gas flow time t. In the temperature range between 350 and 725 °C, these thin films are reduced and oxidized in an ultrafast manner under the flow of H₂ and O₂ gases, respectively, suggesting that PBCC thin films are promising candidates for developing ultra-sensitive oxygen sensors or SOFC cathodes at intermediate or high temperatures. When the gas flow is switched to O₂, the reduced PBCC thin films exhibit a negative resistance at temperatures above 600 °C but a positive resistance at temperatures below 600 °C. The probable cause for these anomalous transport properties is the diffusion of the H atoms from the cathode to the anode in the PBCC film, which provides a current opposite to that resulting from the external voltage.

Keywords: double-perovskite oxide; thin film; oxygen sensing; negative resistance

1. Introduction

In recent years, mixed ionic/electronic conducting materials have attracted much attention because of their potential applications as electrodes in solid oxide fuel cells (SOFCs), ion-transport membranes, and chemical sensors [1–3]. For the development of highly efficient and effective technologies, ultra-sensitive gas sensors/actuators and intermediate-temperature SOFCs are vital. One of the simplest and most easily fabricated sensors is a chemical sensor based on resistance change. Various semiconducting metal oxides such as Fe₂O₃/MoO₃ [4], ZnO [5], and TiO₂ [6] are used as gas sensors. These materials usually require a catalyst such as Co to improve their sensor performance, and their performance at high temperatures is uncertain. Hence, it is important to search for new chemical sensor materials operating in a wide range of temperatures.

Perovskite oxides exhibit mixed ionic/electronic conducting behaviors and unique magnetic, electrical transport, and optical properties. Thus, they are utilized in SOFCs and batteries and for gas sensing and gas separation [7–10]. Moreover, perovskite oxides can accommodate a wide variety of dopants, providing flexibility for controlling the

transport properties. Double perovskites, $AA'B_2O_{5+\delta}$, (A = lanthanide metal, A' = alkaline earth metal, B = transition metal) are very flexible in tailoring various properties [11–14]. The double perovskites $\text{LnBaCo}_2\text{O}_{5+\delta}$ (LnBCO) ($\text{Ln} = \text{La, Pr, Nd}$) possess high catalytic, fast oxygen diffusion, and unique electronic transport properties [15–18]. The physical properties of LnBCO are strongly affected by the oxygen vacancy because it allows for various oxidation states of cobalt ($\text{Co}^{2+}/\text{Co}^{3+}/\text{Co}^{4+}$) and electronic spin states [19]. LnBCO thin films exhibit superfast oxygen redox reactions and thermodynamic stability in a wide range of temperatures. $\text{LaBaCo}_2\text{O}_{5+\delta}$ thin films show a superfast change in the resistance ($3 \times 10^7 \Omega \text{ s}^{-1}$) when the gas flow over the films is switched from H_2 to O_2 in the temperature range between 260–700 °C [20,21]; as do $\text{PrBaCo}_2\text{O}_{5.5+\delta}$ thin films in the temperature range between 200–800 °C [22]. The oxygen vacancy exchange diffusion was found to take place layer-by-layer with a high diffusion rate in $\text{ErBaCo}_2\text{O}_{5.5+\delta}$ thin films [23].

The transport/catalytic properties and the ionic/electronic conductivities of double perovskites $AA'B_2O_{5+\delta}$ are modified when the cation sites are doped with other elements [24–27]. Doping the Co site of $\text{PrBaCo}_2\text{O}_{5+\delta}$ with other transition metals decreases the thermal expansion coefficient [28–31], affecting the electrocatalytic performance [32] and the electrical conductivity [31]. Most studies on $\text{PrBaCo}_2\text{O}_{5+\delta}$ are focused on doping the Co sites, but only a few on the Pr and Ba sites. The electrical transport and magnetic properties of double perovskites $\text{PrBaCo}_2\text{O}_{5+\delta}$ are affected when the Ba sites are doped with various divalent cations, most likely because they increase the oxygen vacancy concentration. Highly epitaxial thin films of $\text{Pr}(\text{Ba}_{0.5}\text{Sr}_{0.5})(\text{Co}_{1.5}\text{Fe}_{0.5})\text{O}_{5.5+\delta}$ exhibit a fast change in resistance under the switching flow of O_2 and H_2 [33]. Both the electron affinity and the redox stability of $\text{PrBaCo}_2\text{O}_{5+\delta}$ are enhanced by the partial doping of the Ba site with Ca [34]. The magnetic and electronic transport properties measured for thin films of $\text{PrBa}_{1-x}\text{Ca}_x\text{Co}_2\text{O}_{5+\delta}$ ($x = 0, 0.3, \text{ and } 0.5$) grown on (001) SrTiO_3 depend on the doping concentration x [35]. In the present work, we carried out a systematic study on the charge transport and the redox dynamics of epitaxial thin films of $\text{PrBa}_{0.7}\text{Ca}_{0.3}\text{Co}_2\text{O}_{5+\delta}$ (PBCC) grown on (001) SrTiO_3 under the switching flow of H_2 and O_2 gases in a wide region of temperature. The PBCC thin films reduced under the gas flow of H_2 show the maximum change of $1.87 \times 10^6 \Omega \text{ s}^{-1}$ in resistance when they are exposed to the flowing gas of O_2 at 450 °C, suggesting that these films are an excellent candidate for developing SOFC devices and ultra-sensitive oxygen sensors. Furthermore, at temperatures above 600 °C, the PBCC films reduced under H_2 (hereafter the reduced PBCC films) exhibit a negative resistance when the gas flow is switched to O_2 . We explore a probable cause for this apparently unprecedented observation.

2. Results and Discussion

Structure. The XRD patterns of the pristine PBCC films and those annealed under O_2 at 700 °C for 8 h are presented in (Figure 1). Only the (00 l) peaks are present in the spectra, indicating that both peaks are oriented along the c direction. The peaks of the PBCC films are all located to the right side of the corresponding peaks of the SrTiO_3 substrate. No additional peaks can be seen, suggesting that the films have no other phase or impurity. The peaks located at 25.78° and 46.42° correspond to the (001) and (002) reflections of SrTiO_3 , respectively [35,36]. The peaks of the pristine PBCC thin films are very close to those of the SrTiO_3 substrates (Figure 1a). After the annealing treatment under O_2 , the peaks of the PBCC films become more evident than those of the pristine PBCC film (Figure 1b). The peak positions for all of the (00 l) peaks slightly shift after the annealing process under O_2 at 700 °C. For example, the (002) diffraction peak of the PBCC films shifts from 47.20° to 47.55° after annealing, which indicates that the c -axis lattice constant slightly decreases. Generally, the c -axis lattice constant of the LnBCO film is related to the oxygen vacancy concentration in the thin film; with the decrease in the oxygen vacancy concentration, the c -axis lattice constant also decreases. The results of the XRD θ - 2θ analysis indicate that there is a certain amount of oxygen vacancies in the in situ grown PBCC films.

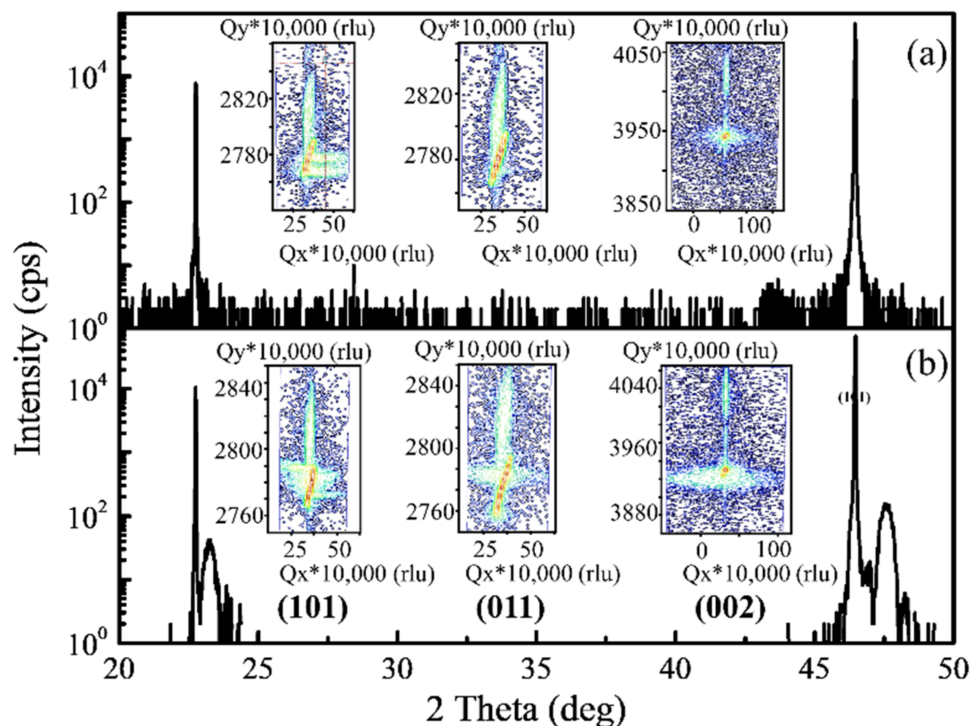


Figure 1. XRD patterns of (a) the as-prepared PBCC film deposited on the (001) SrTiO₃ substrate and (b) the PBCC films after annealing under O₂ at 700 °C for 8 h. The insets are the corresponding RSMs of the as-prepared PBCC film.

The cell parameters determined for the as-prepared PBCC thin films and the films annealed under O₂ at 700 °C, summarized in Table 1, show that the *c*-axis of the annealed films becomes slightly shortened when annealed, indicating that the as-prepared PBCC thin films possess some oxygen vacancies.

Table 1. Lattice constants measured for the thin films of the as-prepared PBCC and the PBCC after annealing under O₂ at 700 °C.

Sample	a (Å)	b (Å)	c (Å)	V(Å ³)
As-prepared PBCC	3.927	3.927	7.660	118.1
Annealed PBCC	3.933	3.933	7.642	118.2

We carried out reciprocal space mapping (RSM) analyses for the PBCC thin films before and after annealing around their symmetric (002) and asymmetric (101) (011) reflections (insets of Figure 1) to obtain the lattice parameters and explore the interface strain of the PBCC films on the SrTiO₃ substrates. The lattice mismatch of the SrTiO₃ substrate and PBCC film is small (~0.56%), indicating that the PBCC film grown on SrTiO₃ has a good crystallinity. The *c*-axis lattice constants of the PBCC films are slightly smaller than two times their *a*-axis lattice constants. After annealing under O₂, the *c*-axis lattice constant decreases, in agreement with the XRD results and the PBCC film expands along the *a*-axis, while maintaining unit cell volumes, which remain effectively unchanged.

Resistance of the as-prepared PBCC films. The temperature-dependent electrical resistance of the as-grown PBCC thin films is shown in Figure 2. The resistance is reversible during the cooling/heating processes. However, there is a hysteresis phenomenon, which suggests that the redox reaction in the PBCC thin film is not an equilibrium process. The resistance of the PBCC thin films increases with decrease in temperature from 750 to 100 °C (Figure 2). In the higher temperature range of 350–750 °C, the ln(ρ /T) vs. 1/T plot is

practically linear (the inset of Figure 2) and is well described by Equation (1) based on the small polaron hopping model [37]:

$$\rho = CT\exp\left(\frac{E_a}{k_B T}\right), \quad (1)$$

where k_B is Boltzmann constant, and E_a the activation energy. From the linear plot in the inset of Figure 2 and Equation (1), E_a is 0.265 eV. The small polaron hopping mechanism is attributed to the presence of mixed-valence states of Co^{3+} and Co^{4+} in the PBCC thin films. The latter has a good thermal stability and a simple activation behavior in the temperature range of 350–750 °C without any clear lattice change, even at 750 °C [38].

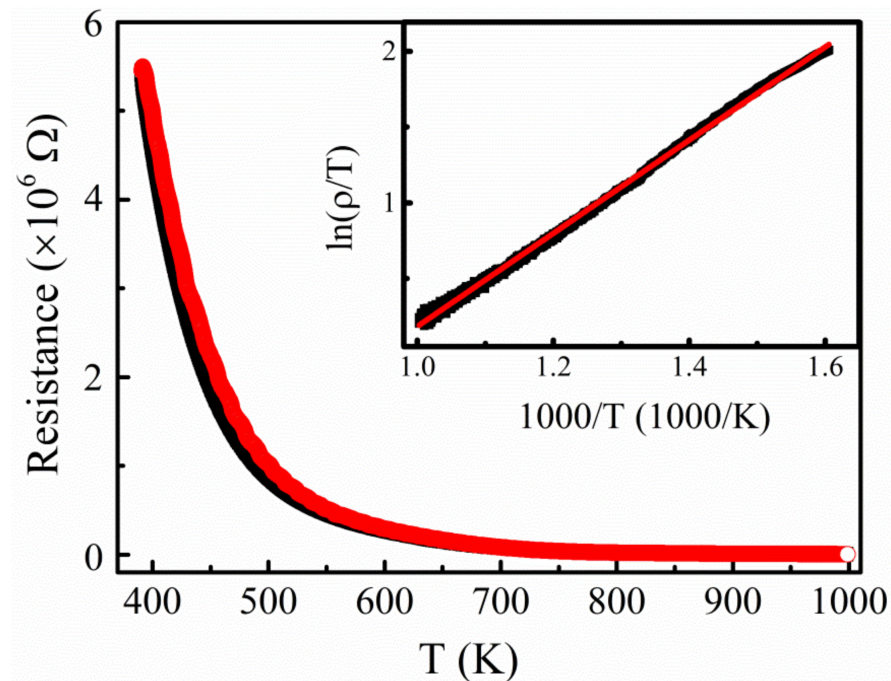


Figure 2. Temperature dependence of electrical resistivity of PBCC film in the oxygen atmosphere from 100 °C to 750 °C (373–1023 K); The inset is the relation of $\ln(\rho/T)$ vs. $1000/T$ of PBCC film in the oxygen atmosphere from 350 °C to 750 °C (623–1023 K).

Redox reactions of PBCC thin films at 450 °C. We first explore the oxygen/hydrogen diffusion behavior of the PBCC films under the switching-flow reducing gas, H_2 , and oxidizing gas, O_2 , at 450 °C by measuring the resistance $R(t)$ as a function of the gas flow time t . As a representative case, we consider the results obtained at 450 °C. The resistance $R(t)$ vs. t and its associated $dR(t)/dt$ vs. t curves under the switching gas for cycles are shown in Figure 3a. The $R(t)$ vs. t curve indicates the excellent stability of the PBCC films. A zoomed-in view of the $R(t)$ vs. t and the corresponding $dR(t)/dt$ vs. t plots for a single oxidation/reduction cycle is shown in Figure 3b. As the gas flow is switched from O_2 to H_2 , the resistance gradually increases to the maximum and then decreases quickly until it reaches the equilibrium value. When switching back to O_2 , the resistance increases rapidly to the maximum and subsequently decreases to the equilibrium value. This two-stage change in the resistance occurs in both the reducing and oxidizing atmospheres.

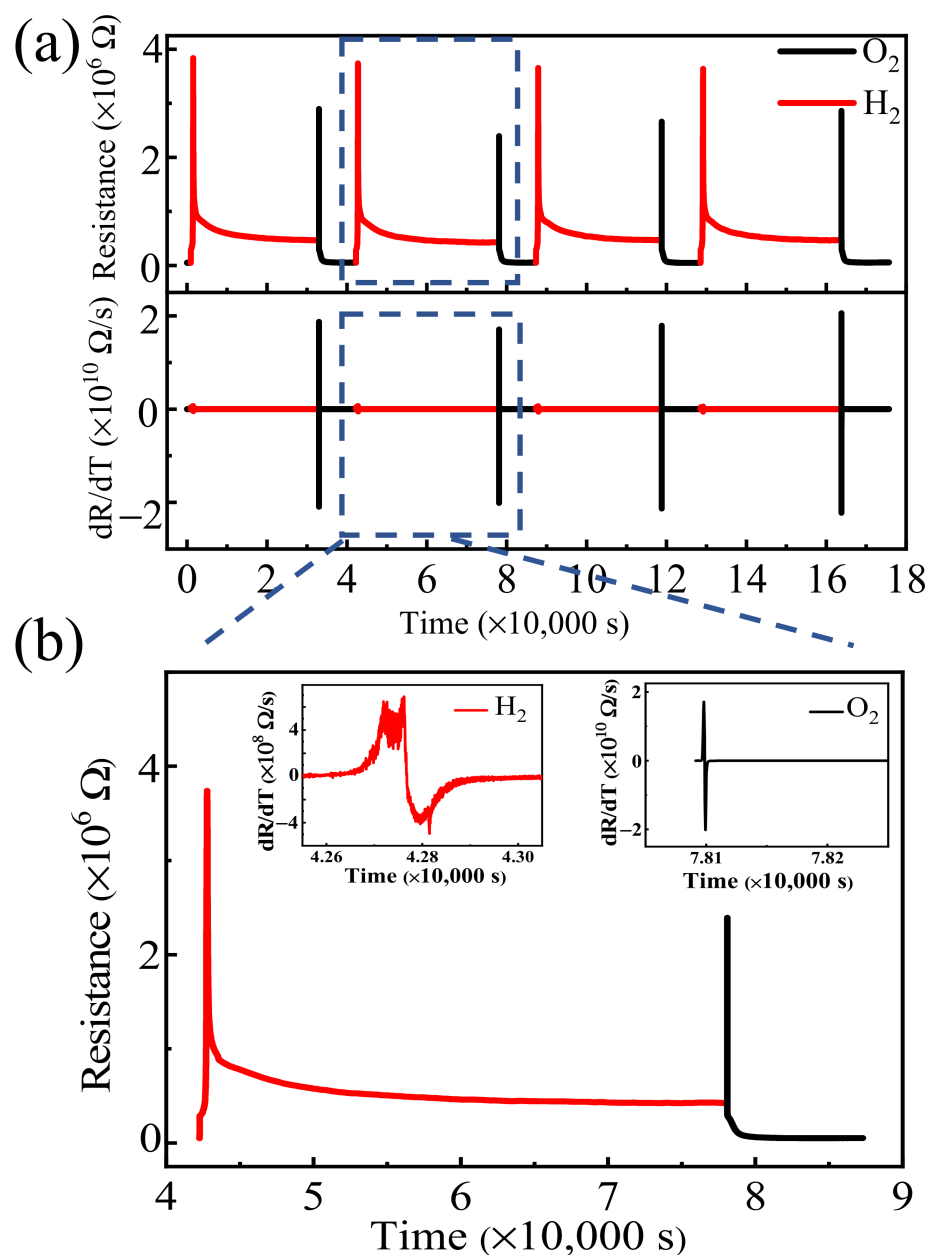


Figure 3. (a) $R(t)$ vs. t and the corresponding $dR(t)/dt$ vs. t curves of PBCC thin films under oxidizing/reducing atmospheres at 450 °C; (b) A zoomed-in view of the $R(t)$ vs. t curve for one oxidation/reduction cycle, and the insets are the corresponding $dR(t)/dt$ vs. t curves of PBCC thin film under O_2/H_2 .

Negative resistance of reduced PBCC thin films during oxidation. To study the oxygen/hydrogen diffusion behavior of the PBCC films in more detail, the $R(t)$ vs. t curves of the PBCC thin films at various temperatures (725, 700, 650, 600, 550 and 350 °C) are compared in Figure 4. The reduction and oxidation processes of the PBCC films are also highly reversible under H_2 and O_2 gases at each temperature, confirming the superior structural stability of PBCC films in the temperature range of 350–725 °C. The two-stage change in the resistance occurs at all specific temperatures under both the reducing and oxidizing atmosphere. When the gas flow is switched from H_2 to O_2 , the PBCC films show a positive resistance at temperatures below 600 °C but a negative resistance at temperatures above 600 °C. The latter observation is anomalous because electrons normally flow from the cathode to the anode under the external voltage V_a (>0) applied to the two electrodes

(Figure 5a). The occurrence of a negative resistance means that electron flows from the anode to the cathode rather than from the cathode to the anode. A key to understanding this unprecedented observation is that the current flowing in the external circuit is governed not only by the external voltage V_a but also by the “internal voltage” between the cathode and anode within the PBCC film. The latter is generated when the PBCC film around the cathode becomes different in chemical composition from that around the anode. In what follows, we explore a probable cause for this anomalous resistance of the reduced PBCC thin films.

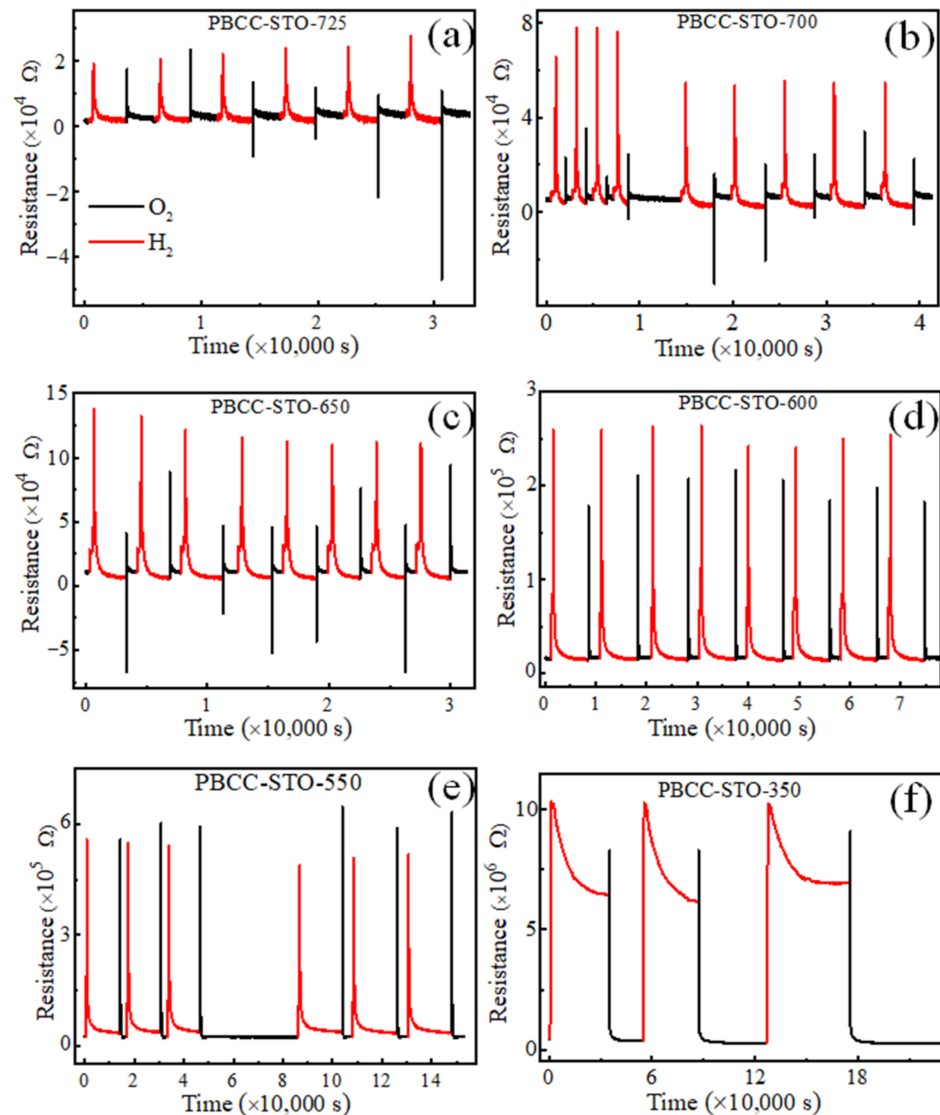


Figure 4. $R(t)$ vs. t curves of PBCC thin films grown on (001) STO, while switching the flow of H₂ and O₂ gases at various temperatures (725, 700, 650, 600, 550, and 350 °C), which are corresponding to the subfigure (a–f), respectively.

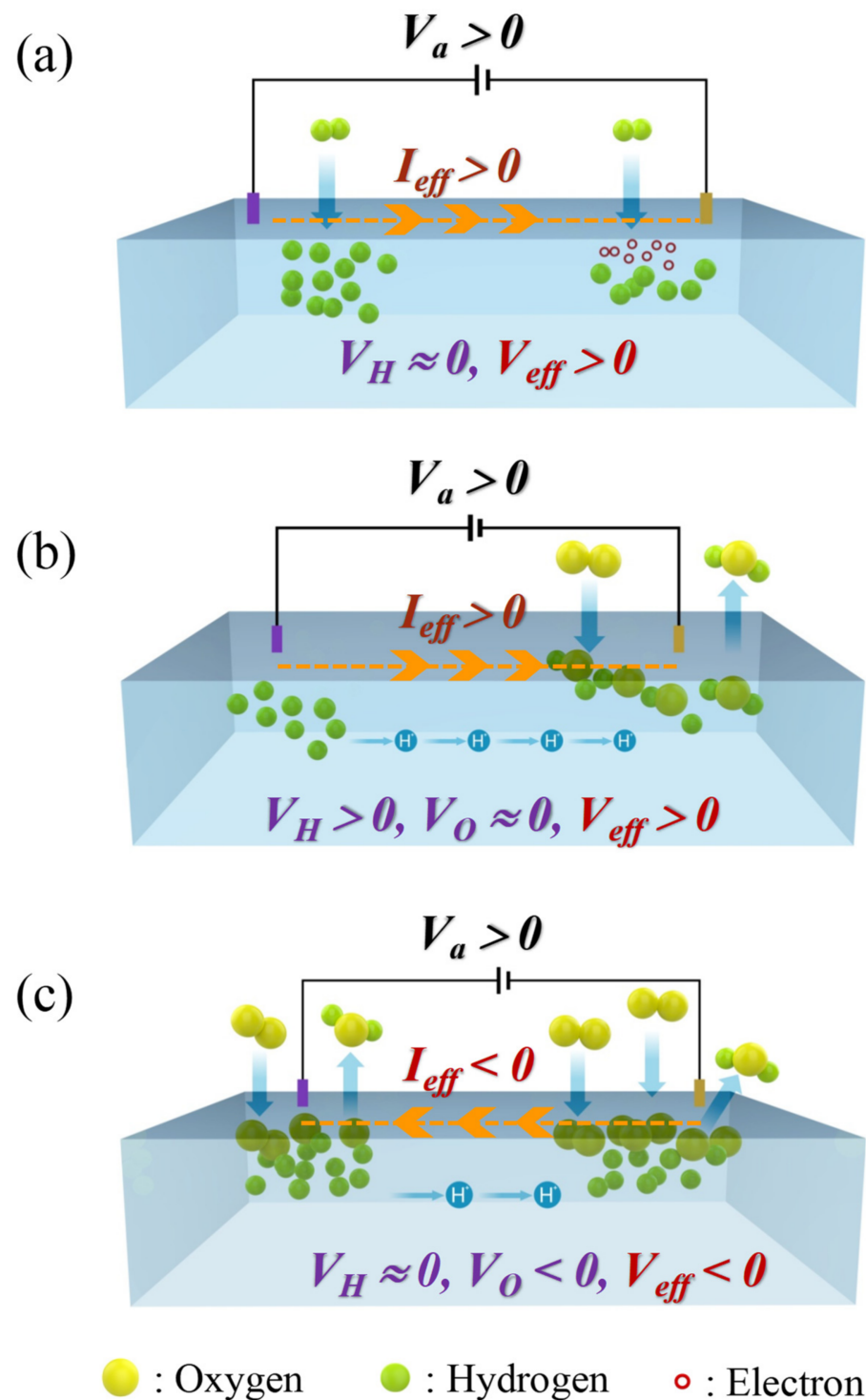


Figure 5. (a) PBCC thin film under the reducing gas, H_2 gas. (b) Reduced PBCC thin film under O_2 gas at temperatures below $600\text{ }^\circ\text{C}$. (c) Reduced PBCC thin film under O_2 gas at temperatures above $600\text{ }^\circ\text{C}$.

Cause for the negative resistance. In the absence of either reducing or oxidizing gas, the current I_a flows from the cathode to the anode under the external voltage $V_a > 0$. Under the H_2 gas, the surface region of the PBCC thin film is reduced. The H_2 molecules are dissociated into the H atoms (with the bond dissociation energy of 104 kcal/mol), which are diffused into the perovskite lattice. It is most likely that the H atoms are ionized

(i.e., $\text{H} \rightarrow \text{H}^+ + \text{e}^-$) to become H^+ cations, which become attached to the O^{2-} ions of the perovskite framework, while the electrons released are accumulated in the vicinity of the anode (Figure 5a). The dissociation of H_2 molecules and the subsequent ionization of the H atoms occur in all parts on the surface of the PBCC thin film. However, there will be slightly fewer H^+ ions in the vicinity of the anode because more electrons are present, and thus they disfavor the ionization of H. The diffusion of H^+ ions between the two electrode leads to an internal current between them so that the effective current I_{eff} flowing in the external circuit becomes different from I_a . The change from I_a to I_{eff} can be viewed as resulting from the corresponding change in the external voltage from V_a to $V_{\text{eff}} = V_a + V_{\text{H}}$, where V_{H} is the internal voltage associated with the H^+ ion diffusion. At the end of the flowing H_2 gas flow, there is practically no diffusion of H^+ ions between the electrodes, so that $V_{\text{H}} \approx 0$. Then, $V_{\text{eff}} = V_a + V_{\text{H}} \approx V_a > 0$, leading to a positive resistance.

Now we consider what happens when the reduced PBCC thin film under H_2 gas is exposed to the O_2 gas flow. The two O atoms resulting from the dissociation of O_2 (with the bond dissociation energy of 119 kcal/mol) can receive electrons from the PBCC film to become two O^{2-} anions. It is in the vicinity of the anode where the ionization, $\text{O} + 2\text{e}^- \rightarrow \text{O}^{2-}$, is favored because electrons are more abundant there than in the vicinity of the cathode. Suppose that the dissociation of O_2 and the subsequent ionization of the O atoms take place primarily in the anode region (Figure 5b). Then, the O^{2-} anions combine with the H^+ ions to form H_2O and leave the PBCC surface from the vicinity of the anode. This results in more H^+ ions in the cathode than in the anode region, which induces the diffusion of the H^+ ions from the cathode to the anode with the associated current in the same direction to that induced by V_a . Hence, the resulting current I_{eff} is larger than I_a ; the effective external voltage $V_{\text{eff}} = V_a + V_{\text{H}}$ is larger than V_a because of $V_{\text{H}} > 0$. The O^{2-} ions generated in the vicinity of the anode leave the surface as H_2O , and thus do not affect the effective voltage V_{eff} ; the contribution of O^{2-} ions to the effective external voltage, V_{O} , is negligibly small ($V_{\text{O}} \approx 0$). As long as $V_{\text{eff}} = V_a + V_{\text{H}} + V_{\text{O}} > 0$, the effective current I_{eff} is positive, as is the effective resistance.

In the above, we considered the dissociation of O_2 preferentially around the anode, since the electrons needed for the ionization of O are more abundant there. In general, such selectivity of the reaction is favorable at low temperatures. At high temperatures, the O_2 dissociation becomes easier, and thus occurs almost equally around the two electrodes on the PBCC film surface (Figure 5c). Since more electrons are present in the vicinity of the anode, more O^{2-} ions are present there than in the cathode region. Since there are less H^+ ions in the anode region, the formation of H_2O depletes H^+ ions more quickly in the anode region unless diffusions of H^+ and O^{2-} ions occur between the electrodes. This is the case at high temperatures because the perovskite oxygen atoms vibrate strongly, acting as scatterers for ionic species diffusing between the two electrodes. This could result in more O^{2-} ions in the anode than in the cathode region. The latter might raise the energy states of the PBCC around the anode region above those around the cathode region, thereby reversing the sign of the effective voltage, i.e., $V_{\text{eff}} = V_a + V_{\text{H}} + V_{\text{O}} < 0$, which is possible if V_{O} is substantially negative. This leads to a negative resistance.

In short, the case of Figure 5b explains the observation of positive resistance below 600 °C, and that of Figure 5c the observation of negative resistance above 600 °C. If this explanation is correct, a negative resistance will not occur if V_a dominates over V_{H} and V_{O} , provided that the applied voltage V_a is large enough. In agreement with this prediction, we note that the reduced PBCC exhibits a negative resistance to temperatures above 600 °C when $V_a = 0.2$ V. When V_a is raised to 1.0 V, the PBCC thin film does not exhibit a negative resistance (see Supplementary Materials Figure S1).

Different redox reactions at various temperatures. The detailed processes of the redox reactions of PBCC thin films at 650, 600, 550, and 400 °C are shown in Supplementary Materials Figure S2. The two-stage changes of the resistance can be seen under both the reducing and oxidizing atmospheres due to the change in the valence of the Co ions. The resistance $R(t)$ vs. t and its associated $dR(t)/dt$ vs. t curves under O_2 or H_2 for a single

process at specific temperatures are shown in Figures S3 and S4, respectively. The rate of the resistance change under O₂ is far greater than that under H₂, suggesting the excellent oxygen sensitivity of the reduced PBCC films. Upon switching to O₂, the resistance of the PBCC films shows a drastic change within 2 s, displaying a superior oxygen sensing performance, compared to most oxides (Table 2) [39–45].

Table 2. Features of medium- and high-temperature oxygen sensors based on various semiconductor oxides.

Oxide	Response Time (s) (t _{90%})	Temperature (°C)	Ref
1.5 wt% Zn-doped SnO ₂	141	250	[39]
CdO-ZnO hexagonal particles	43	200	[40]
CdO:ZnO (3:1) nanostructure	18	32–200	[41]
CdO:ZnO (3:1) nanocomposite thin film	10–20	25–200	[42]
Ti ₃ O ₅	67	200	[43]
VO _x /TiO ₂	3–5	100	[44]
(LaBa)Co ₂ O _{5+δ} thin film	~2.2	580	[45]
PrBa _{0.7} Ca _{0.3} Co ₂ O _{5+δ} thin film	<2	350–725	This work

3. Materials and Methods

PBCC thin films were epitaxially grown on (001) SrTiO₃ by pulsed laser deposition (PLD). Similar to the other LnBCO thin film preparations [35,46], a KrF excimer pulsed-laser deposition system with a wavelength of 248 nm was employed to grow the PBCC films on an (001) STO substrate. Similar to the other LnBCO epitaxial film growth, the optimal growth conditions were determined to be at a deposition temperature of 850 °C and an oxygen pressure of 100 mTorr with a laser energy density of 1.5–2.0 J/cm². The film thicknesses were about 60 nm measured by using a step gauge. Soon after deposition, the PBCC films were in situ annealed at 850 °C for 15 min in a pure oxygen atmosphere at 200 Torr and slowly cooled to room temperature with a rate of 5 °C/min. The X-ray diffraction (XRD) was conducted using PANalytical X-ray Diffractometer with Cu K α radiation ($\lambda = 0.15418$ nm) to characterize the crystallinity of the PBCC films. To study the electrical and oxidizing/reducing properties of the PBCC films, the AC conductivity measurements were carried out using the Lake Shore 370 AC Bridge in the temperature region between 350–725 °C, with an atmosphere of pure oxygen (O₂) or a mixture of 4% hydrogen and 96% nitrogen (referred to as H₂ in this work) at 1 atm. As the electrodes for the resistance measurements, we glued two platinum leads on the PBCC film surface with silver paste, which were dried in air at room temperature and were then annealed at 700 °C under O₂.

4. Conclusions

We prepared thin films of Ca-doped double perovskite, PrBa_{0.7}Ca_{0.3}Co₂O_{5+δ} (PBCC), on (001) SrTiO₃ and investigated their redox behaviors under a switching flow of H₂ and O₂ gases to find that these films were reduced and oxidized in an ultrafast manner under the flowing gas of H₂ and O₂, respectively. When exposed to the gas flow of O₂, the reduced PBCC films showed a normal transport behavior at temperatures below 600 °C but an apparently anomalous behavior at temperatures above 600 °C. That is, their resistance was positive below 600 °C, but negative above 600 °C. This anomalous transport property is explained by considering the effect of the H atom diffusion from the cathode to the anode, which is caused by the reduction taking place around the anode. Our work suggests that PBCC thin films are promising candidates for developing ultra-sensitive oxygen sensors or SOFC cathodes at intermediate or high temperatures.

Supplementary Materials: The following are available online at <https://www.mdpi.com/article/10.3390/catal11121441/s1>. Figure S1. R(t) vs. t curves of PBCC thin films grown on (001) STO with switching the flow of H₂ and O₂ gases at 700 °C when applied potential is set as 1.0 V. Figure S2. Single redox processes of PBCC thin films grown on STO with switching the flow of H₂ and O₂ gases at various temperatures (650, 600, 550, and 400 °C). Figure S3. R(t) vs. t and dR(t)/dt vs. t of the epitaxial PBCC thin film under O₂ at various temperatures. Figure S4. R(t) vs. t and dR(t)/dt vs. t of the epitaxial PBCC thin film under H₂ at various temperatures.

Author Contributions: Y.L. and C.C. designed the study. C.C. overseas the project. X.X., Y.X., and S.P. helped perform the experiments. Y.L., M.-H.W. and C.C. wrote the paper and conceived the theoretical model. Y.L., X.X., Y.X., S.P., F.X., M.-H.W., L.S., C.C. reviewed and edited the manuscript. All authors have read and agreed to the published version of the manuscript.

Funding: This research was funded by the UTSA seed research fund, National Natural Science Foundation of China [51871065], the study abroad program for the graduate students of Guilin University of Electronic Technology [YXYJ2900].

Institutional Review Board Statement: Not applicable.

Informed Consent Statement: Not applicable.

Data Availability Statement: The data presented in this study are openly available via MDPI.

Acknowledgments: This work was partially supported by the UTSA seed research fund, National Natural Science Foundation of China [51871065], the study abroad program for graduate students of Guilin University of Electronic Technology [YXYJ2900].

Conflicts of Interest: The authors declare no conflict of interest.

References

1. Zeng, Q.N.; Zhang, X.Z.; Wang, W.; Zhang, D.D.; Jiang, Y.H.; Zhou, X.J.; Lin, B. A Zn-Doped Ba_{0.5}Sr_{0.5}Co_{0.8}Fe_{0.2}O_{3-δ} Perovskite Cathode with Enhanced ORR Catalytic Activity for SOFCs. *Catalysts* **2020**, *10*, 235. [\[CrossRef\]](#)
2. Chen, H.; Li, L.J.; Kemps, R.; Michielsen, B.; Jacobs, M.; Snijkers, F.; Middelkoop, V. Reactive air brazing for sealing mixed ionic electronic conducting hollow fibre membranes. *Acta Mater.* **2015**, *88*, 74–82. [\[CrossRef\]](#)
3. Khandale, A.P.; Pahune, B.S.; Bhoga, S.S.; Kumar, R.V.; Tomov, R. Development of Pr_{2-x}Sr_xCuO_{4+δ} mixed ion-electron conducting system as cathode for intermediate temperature solid oxide fuel cell. *Int. J. Hydrogen Energy* **2019**, *44*, 15417–15435. [\[CrossRef\]](#)
4. Qu, F.; Zhou, X.; Zhang, B.; Zhang, S.; Jiang, C.; Ruan, S.; Yang, M. Fe₂O₃ nanoparticles-decorated MoO₃ nanobelts for enhanced chemiresistive gas sensing. *J. Alloys Compd.* **2019**, *782*, 672–678. [\[CrossRef\]](#)
5. Hagedorn, K.; Li, W.; Liang, Q.; Dilger, S.; Noebels, M.; Wagner, M.R.; Reparaz, J.S.; Dollinger, A.; Guenne, J.S.A.D.; Dekorsy, T.; et al. Catalytically Doped Semiconductors for Chemical Gas Sensing: Aerogel-Like Aluminum-Containing Zinc Oxide Materials Prepared in the Gas Phase. *Adv. Funct. Mater.* **2016**, *26*, 3424–3437. [\[CrossRef\]](#)
6. Shi, C.; Rani, A.; Thomson, B.; Debnath, R.; Motayed, A.; Ioannou, D.E.; Li, Q. High-performance room-temperature TiO₂-functionalized GaN nanowire gas sensors. *Appl. Phys. Lett.* **2019**, *115*, 121602. [\[CrossRef\]](#)
7. Shen, Q.W.; Dong, S.S.; Li, S.; Yang, G.G.; Pan, X.X. A Review on the Catalytic Decomposition of NO by Perovskite-Type Oxides. *Catalysts* **2021**, *11*, 622. [\[CrossRef\]](#)
8. Joo, S.; Kwon, O.; Kim, K.; Kim, S.; Kim, H.; Shin, J.; Jeong, H.Y.; Sengodan, S.; Han, J.W.; Kim, G. Cation-swapped homogeneous nanoparticles in perovskite oxides for high power density. *Nat. Commun.* **2019**, *10*, 697. [\[CrossRef\]](#)
9. Lin, Y.S.; Choi, E.M.; Lu, P.; Sun, X.; Wu, R.; Yun, C.; Zhu, B.N.; Wang, H.Y.; Li, W.W.; Maity, T.; et al. Vertical Strain-Driven Antiferromagnetic to Ferromagnetic Phase Transition in EuTiO₃ Nanocomposite Thin Films. *ACS Appl. Mater. Interfaces* **2020**, *12*, 8513–8521. [\[CrossRef\]](#)
10. Gao, Y.; Wang, J.J.; Wu, L.; Bao, S.Y.; Shen, Y.; Lin, Y.H.; Nan, C.W. Tunable magnetic and electrical behaviors in perovskite oxides by oxygen octahedral tilting. *Sci. China Mater.* **2015**, *58*, 302–312. [\[CrossRef\]](#)
11. Chen, M.F.; Bao, S.Y.; Zhang, Y.; Wang, Y.J.; Liang, Y.H.; Wu, J.L.; Huang, T.T.; Wu, L.; Yu, P.; Zhu, J.; et al. Physical and chemical strains co-tuned magnetic properties of double perovskite PrBaMn₂O_{5+δ} epitaxial films. *Appl. Phys. Lett.* **2019**, *115*, 081903. [\[CrossRef\]](#)
12. Kim, S.; Jun, A.; Kwon, O.; Kim, J.; Yoo, S.; Jeong, H.Y.; Shin, J.; Kim, G. Nanostructured Double Perovskite Cathode with Low Sintering Temperature For Intermediate Temperature Solid Oxide Fuel Cells. *ChemSuschem* **2015**, *8*, 3153–3158. [\[CrossRef\]](#) [\[PubMed\]](#)
13. Hua, B.; Zhang, Y.Q.; Yan, N.; Li, M.; Sun, Y.F.; Chen, J.; Li, J.; Luo, J.L. The Excellence of Both Worlds: Developing Effective Double Perovskite Oxide Catalyst of Oxygen Reduction Reaction for Room and Elevated Temperature Applications. *Adv. Funct. Mater.* **2016**, *26*, 4106–4112. [\[CrossRef\]](#)

14. Zhu, Y.; Zhang, L.; Zhao, B.; Chen, H.; Liu, X.; Zhao, R.; Wang, X.; Liu, J.; Chen, Y.; Liu, M. Improving the Activity for Oxygen Evolution Reaction by Tailoring Oxygen Defects in Double Perovskite Oxides. *Adv. Funct. Mater.* **2019**, *29*, 1901783. [[CrossRef](#)]
15. Chen, T.; Zhao, H.; Xie, Z.; Xu, N.; Lu, Y. Oxygen permeability of $\text{Ce}_{0.8}\text{Sm}_{0.2}\text{O}_{2-\delta}$ -aEuro parts per thousand $\delta\text{-LnBaCo}_2\text{O}_{(5+\delta)}$ ($\text{Ln}=\text{La}, \text{Nd}, \text{Sm}, \text{and Y}$) dual-phase ceramic membranes. *Ionics* **2015**, *21*, 1683–1692. [[CrossRef](#)]
16. Jia, Z.; Wang, P.; Zhong, Y.; Mei, H. Optimization and Electrochemical Properties of Double Perovskite $\text{NdBaCo}_2\text{O}_{6-(\delta)}$ $\text{LaBaCo}_2\text{O}_{5+\delta}$ as Cathode Material for Solid Oxide Fuel Cell. *J. Nanoelectron. Optoelectron.* **2018**, *13*, 749–757. [[CrossRef](#)]
17. Zhang, L.; Li, S.; Xia, T.; Sun, L.; Huo, L.; Zhao, H. Co-deficient $\text{PrBaCo}_{2-x}\text{O}_{6-\delta}$ perovskites as cathode materials for intermediate-temperature solid oxide fuel cells: Enhanced electrochemical performance and oxygen reduction kinetics. *Int. J. Hydrogen Energ.* **2018**, *43*, 3761–3775. [[CrossRef](#)]
18. Kong, X.; Feng, S.; Sun, H.; Yi, Z.; Liu, G. Effect of Mn on the Characterization of Layered Perovskite $\text{NdBaCo}_{2-x}\text{Mn}_x\text{O}_{5+\delta}$ ($x = 0.5, 1, 1.5, 2$) as Cathode Materials for IT-SOFCs. *Int. J. Electrochem. Sci.* **2018**, *13*, 7939–7948. [[CrossRef](#)]
19. Bernuy-Lopez, C.; Hoydalsvik, K.; Einarsrud, M.-A.; Grande, T. Effect of A-Site Cation Ordering on Chemical Stability, Oxygen Stoichiometry and Electrical Conductivity in Layered $\text{LaBaCo}_2\text{O}_{5+\delta}$ Double Perovskite. *Materials* **2016**, *9*, 154. [[CrossRef](#)]
20. Wang, H.B.; Bao, S.Y.; Liu, J.; Collins, G.; Ma, C.R.; Liu, M.; Chen, C.L.; Dong, C.; Whangbo, M.H.; Guo, H.M.; et al. Ultrafast chemical dynamic behavior in highly epitaxial $\text{LaBaCo}_2\text{O}_{5+\delta}$ thin films. *J. Mater. Chem. C* **2014**, *2*, 5660–5666. [[CrossRef](#)]
21. Liu, J.; Collins, G.; Liu, M.; Chen, C. Superfast oxygen exchange kinetics on highly epitaxial $\text{LaBaCo}_2\text{O}_{5+\delta}$ thin films for intermediate temperature solid oxide fuel cells. *Appl. Mater.* **2013**, *1*, 031101. [[CrossRef](#)]
22. Bao, S.; Xu, X.; Enriquez, E.; Mace, B.E.; Chen, G.; Kelliher, S.P.; Chen, C.; Zhang, Y.; Whangbo, M.-H.; Dong, C.; et al. Atomically layer-by-layer diffusion of oxygen/hydrogen in highly epitaxial $\text{PrBaCo}_2\text{O}_{5.5+\delta}$ thin films. *Appl. Phys. Lett.* **2015**, *107*, 243903. [[CrossRef](#)]
23. Bao, S.; Ma, C.; Chen, G.; Xu, X.; Enriquez, E.; Chen, C.; Zhang, Y.; Bettis, J.L., Jr.; Whangbo, M.-H.; Dong, C.; et al. Ultrafast Atomic Layer-by-Layer Oxygen Vacancy-Exchange Diffusion in Double-Perovskite $\text{LnBaCo}_2\text{O}_{(5.5+\delta)}$ Thin Films. *Sci. Rep.* **2014**, *4*, 4726. [[CrossRef](#)] [[PubMed](#)]
24. Qi, H.; Thomas, T.; Li, W.Y.; Li, W.; Xia, F.; Zhang, N.; Sabolsky, E.M.; Zondlo, J.; Hart, R.; Liu, X.B. Reduced Thermal Expansion and Enhanced Redox Reversibility of $\text{La}_{0.5}\text{Sr}_{1.5}\text{Fe}_{1.5}\text{Mo}_{0.5}\text{O}_{6-\delta}$ Anode Material for Solid Oxide Fuel Cells. *ACS Appl. Energy Mater.* **2019**, *2*, 4244–4254. [[CrossRef](#)]
25. Bu, Y.F.; Gwon, O.; Nam, G.; Jang, H.; Kim, S.; Zhong, Q.; Cho, J.; Kim, G. A Highly Efficient and Robust Cation Ordered Perovskite Oxide as a Bifunctional Catalyst for Rechargeable Zinc-Air Batteries. *ACS Nano* **2017**, *11*, 11594–11601. [[CrossRef](#)]
26. Opherden, L.; Sieger, M.; Pahlke, P.; Huhne, R.; Schultz, L.; Meledin, A.; Van Tendeloo, G.; Nast, R.; Holzappel, B.; Bianchetti, M.; et al. Large pinning forces and matching effects in $\text{YBa}_2\text{Cu}_3\text{O}_{7-\delta}$ thin films with $\text{Ba}_2\text{Y}(\text{Nb}/\text{Ta})\text{O}_6$ nano-precipitates. *Sci. Rep.* **2016**, *6*, 21188. [[CrossRef](#)] [[PubMed](#)]
27. Kleibeuker, J.E.; Choi, E.-M.; Jones, E.D.; Yu, T.-M.; Sala, B.; MacLaren, B.A.; Kepaptsoglou, D.; Hernandez-Maldonado, D.; Ramasse, Q.M.; Jones, L.; et al. Route to achieving perfect B-site ordering in double perovskite thin films. *NPG Asia Mater.* **2017**, *9*, 406. [[CrossRef](#)]
28. Jin, F.; Li, J.; Wang, Y.; Chu, X.; Xu, M.; Zhai, Y.; Zhang, Y.; Fang, W.; Zou, P.; He, T. Evaluation of Fe and Mn co-doped layered perovskite $\text{PrBaCo}_2/3\text{Fe}_2/3\text{Mn}_1/2\text{O}_{5+\delta}$ as a novel cathode for intermediate-temperature solid-oxide fuel cell. *Ceram. Int.* **2018**, *44*, 22489–22496. [[CrossRef](#)]
29. Huang, X.; Feng, J.; Abdellatif, H.R.S.; Zou, J.; Zhang, G.; Ni, C. Electrochemical evaluation of double perovskite $\text{PrBaCo}_{2-x}\text{Mn}_x\text{O}_{(5+\delta)}$ ($x = 0, 0.5, 1$) as promising cathodes for IT-SOFCs. *Int. J. Hydrogen Energ.* **2018**, *43*, 8962–8971. [[CrossRef](#)]
30. Enriquez, E.; Chen, A.; Harrell, Z.; Dowden, P.; Koskelo, N.; Roback, J.; Janoschek, M.; Chen, C.; Jia, Q. Oxygen Vacancy-Tuned Physical Properties in Perovskite Thin Films with Multiple B-site Valance States. *Sci. Rep.* **2017**, *7*, 46184. [[CrossRef](#)]
31. Guo, W.; Guo, R.; Liu, L.; Cai, G.; Zhang, C.; Wu, C.; Liu, Z.; Jiang, H. Thermal and electrochemical properties of layered perovskite $\text{PrBaCo}_{2-x}\text{Mn}_x\text{O}_{5+\delta}$ ($x = 0.1, 0.2 \text{ and } 0.3$) cathode materials for intermediate temperature solid oxide fuel cells. *Int. J. Hydrogen Energ.* **2015**, *40*, 12457–12465. [[CrossRef](#)]
32. Saccoccio, M.; Jiang, C.; Gao, Y.; Chen, D.; Ciucci, F. Nb-substituted $\text{PrBaCo}_2\text{O}_{5+\delta}$ as a cathode for solid oxide fuel cells: A systematic study of structural, electrical, and electrochemical properties. *Int. J. Hydrogen Energ.* **2017**, *42*, 19204–19215. [[CrossRef](#)]
33. Enriquez, E.; Xu, X.; Bao, S.; Harrell, Z.; Chen, C.; Choi, S.; Jun, A.; Kim, G.; Whangbo, M.-H. Catalytic Dynamics and Oxygen Diffusion in Doped $\text{PrBaCo}_2\text{O}_{5.5+\delta}$ Thin Films. *ACS Appl. Mater. Interfaces* **2015**, *7*, 24353–24359. [[CrossRef](#)]
34. Pang, S.; Yang, G.; Su, Y.; Xu, J.; Shen, X.; Zhu, M.; Wu, X.; Li, S.; Chen, C. A-site cation deficiency tuned oxygen transport dynamics of perovskite $\text{Pr}_{0.5}\text{Ba}_{0.25-x}\text{Ca}_{0.25}\text{CoO}_{3-\delta}$ oxide for intermediate temperature solid oxide fuel cells. *Ceram. Int.* **2019**, *45*, 14602–14607. [[CrossRef](#)]
35. Bao, S.; Pang, S.; Wang, W.; Chen, J.; Chen, M.; Ma, J.; Nan, C.-W.; Chen, C. Ca doping effect on the magnetic and electronic transport properties in double perovskite $\text{PrBaCo}_2\text{O}_{5+\delta}$ films. *Appl. Phys. Lett.* **2017**, *111*, 232406. [[CrossRef](#)]
36. Fan, M.; Wang, H.; Misra, S.; Zhang, B.; Qi, Z.; Sun, X.; Huang, J.; Wang, H. Microstructure, Magnetic, and Magnetoresistance Properties of $\text{La}_{0.7}\text{Sr}_{0.3}\text{MnO}_3:\text{CuO}$ Nanocomposite Thin Films. *ACS Appl. Mater. Interfaces* **2018**, *10*, 5779–5784. [[CrossRef](#)] [[PubMed](#)]
37. Mukherjee, R.; Dutta, A.; Sinha, T.P. Dielectric Relaxation of Rare Earth Ordered Double Perovskite Oxide $\text{Ba}_2\text{ErTaO}_6$. *J. Electron. Mater.* **2016**, *45*, 846–852. [[CrossRef](#)]

38. Wang, H.; Enriquez, E.; Collins, G.; Ma, C.; Liu, M.; Zhang, Y.; Dong, C.; Chen, C. Anomalous redox properties and ultrafast chemical sensing behavior of double perovskite $\text{CaBaCo}_2\text{O}_{5+\delta}$ thin films. *J. Mater.* **2015**, *1*, 113–117. [[CrossRef](#)]
39. Gupta, P.; Sharma, S.K. A study of oxygen gas sensing in Zn-doped SnO_2 nanostructures. *Mater. Res. Express* **2017**, *4*, 065010. [[CrossRef](#)]
40. Rajput, J.K.; Pathak, T.K.; Kumar, V.; Swart, H.C.; Purohit, L.P. Controlled sol-gel synthesis of oxygen sensing CdO:ZnO hexagonal particles for different annealing temperatures. *RSC Adv.* **2019**, *9*, 31316–31324. [[CrossRef](#)]
41. Rajput, J.K.; Pathak, T.K.; Kumar, V.; Swart, H.C.; Purohit, L.P. CdO:ZnO nanocomposite thin films for oxygen gas sensing at low. *Mater. Sci. Eng. B* **2018**, *228*, 241–248. [[CrossRef](#)]
42. Rajput, J.K.; Pathak, T.K.; Purohit, L.P. Impact of Sputtering Power on Properties of CdO:ZnO Thin Films Synthesized by Composite Method for Oxygen Gas Sensing Application. *J. Electron. Mater.* **2019**, *48*, 6640–6646. [[CrossRef](#)]
43. Zhang, X.; Liu, W.; Yu, H.; Zhong, X.; Wang, L.; Singh, A.; Lin, Y. Preparation and oxygen sensing properties of Ti_3O_5 submicron rods. *Micro Nano Lett.* **2016**, *11*, 811–813. [[CrossRef](#)]
44. Raghu, A.V.; Karuppanan, K.K.; Pullithadathil, B. Highly Sensitive, Temperature-Independent Oxygen Gas Sensor Based on Anatase TiO_2 Nanoparticle Grafted, 2D Mixed Valent VOx Nanoflakelets. *ACS Sens.* **2018**, *3*, 1811–1821. [[CrossRef](#)]
45. Hong, D.; Pan, T.; Feng, D.; Huang, Z.; Liao, F.; Li, X.; Zhang, Y.; Gao, M. The oxygen sensitive properties of $(\text{LaBa})\text{Co}_2\text{O}_{5+\delta}$ thin films fabricated by polymer-assisted deposition technique. *J. Sol-Gel Sci. Technol.* **2014**, *71*, 464–469. [[CrossRef](#)]
46. Yuan, Z.; Liu, J.; Chen, C.L.; Wang, C.H.; Luo, X.G.; Chen, X.H.; Kim, G.T.; Huang, D.X.; Wang, S.S.; Jacobson, A.J.; et al. Epitaxial behavior and transport properties of $\text{PrBaCo}_2\text{O}_5$ thin films on (001) SrTiO_3 . *Appl. Phys. Lett.* **2007**, *90*, 212111. [[CrossRef](#)]